AIAA 78-1358R

Numerical Study of Re-entry Vehicle Aerodynamics in Steady Coning Motion

T.C. Lin*
TRW Defense and Space Systems Group, San Bernardino, Calif.

The objective of the present investigation is to formulate a numerical model to predict the aerodynamics of a hi-speed re-entry vehicle (RV). This analytical model is able to estimate the aerodynamic effects of the rotational motions (e.g., spinning and precession) of the vehicle as well as those effects resulting from its translational motions. Numerical results are presented for the three-dimensional flowfield about a blunt cone in a steady coning motion. The theoretical formulation consists of a two-layer model: the outer inviscid flow and the inner laminar and/or turbulent boundary layers. One significant contribution of the present paper is the estimation of the dynamic stability properties such as pitch- and roll-damping derivatives. Effects of freestream Mach number, vehicle bluntness ratio, angle of attack, and the center of gravity location upon the flow properties are discussed.

Nomenclature

C_{l_p}	= roll-damping derivative
$C_{m_q}+C_{m_{\dot\alpha}}$	= pitch-damping derivative
D	= base diameter
I	= moment of inertia
κ	= thermal conductivity
M	= Mach number or RV mass
p	= pressure
q	= dynamic pressure
R_N	= nosetip radius
(r,θ,ϕ)	= spherical coordinate
S	= entropy
T	= temperature
(u,v,w)	= velocity components in (x,y,z), respectively
x,y,z	= coordinates (see Fig. 1)
α	= angle of attack
δ,Δ	= boundary layer thickness
θ_c	= cone half-angle
μ	= viscosity
Ω	= precession velocity
ω	= spin velocity

Subscripts

cg	= center of gravity location
e	= boundary edge properties
w	= surface condition
∞	= freestream condition

Introduction

DURING the last decade, significant progress has been achieved in the theoretical estimation capability in hypersonic inviscid flows. For example, the sophisticated inviscid subsonic-transonic-supersonic flowfield calculations[1-3] are now being used routinely to evaluate the aerodynamics of the complex three-dimensional missile configurations. However, these flowfield codes are limited in that they are capable of analyzing only those aerodynamic effects resulting from translational motions of the body relative to the surrounding atmosphere. Because the motions of an RV involve both translational and rotational motions, it is desirable to be able to analyze the aerodynamic effects of the rotational motions of the vehicle as well as those effects resulting from its translational motions.

Numerical formulations of Refs. 1-3 are made at constant angle of attack; consequently only static values are evaluated. No account is taken of flow lag. The only exceptions are Refs. 4 and 5. Brong[4] uses a perturbation analysis to expand flow properties in terms of angle of attack α and the pitch frequency qL/U_∞. Only one term in the expansion is used in his formulation. Therefore, Brong's analysis is limited to linear aerodynamics. It is known that the missile aerodynamics can be highly nonlinear on blunt vehicles. Schiff employed a shock-capturing finite-difference technique[5] to calculate the flowfields about bodies in steady coning motion. Numerical results are compared with experimental data,[6] and good agreement is obtained. So far, both Brong and Schiff's formulations are limited to sharp cones in inviscid flow only.

The purpose of this paper is to extend the existing numerical model to the more general vehicle dynamics. Attention is focused on the vehicle with steady coning motion. One significant contribution of this study is the estimation of the dynamic stability properties, such as pitch damping and roll damping, on a blunt cone geometry.

Formulation

Outer Inviscid Flows—Blunt-Nose Region[7]

For missiles undergoing a constant coning motion and a fixed spinning rate, the shock layer is divided into the outer inviscid flow and the inner-boundary-layer flows. The governing equations for the outer flows are the Euler equations, i.e.,

$$\rho_t+\nabla\cdot(\rho V)=0,\quad V_t+(V\cdot\nabla)V+2(\Omega\times V)+\frac{1}{\rho}\nabla p-(\Omega\times r)\times\Omega=-\Omega\times V_{cg} \tag{1}$$

Because Eq. (1) is written in a moving frame of reference, the fluid particles shall experience a Coriolis acceleration and centrifugal force. In the blunt-nose subsonic-transonic flow regimes, a time-dependent relaxation method is used, while downstream supersonic flows are calculated by the streamwise marching technique. The blunt-body calculations are carried out with the following basic equations written in spherical coordinates (see Fig. 1 for notation):

Continuity:

$$\rho_t+\frac{1}{r^2}\frac{\partial}{\partial r}(\rho ur^2)+\frac{1}{r\sin\theta}\frac{\partial}{\partial\theta}(\rho v\sin\theta)+\frac{1}{r\sin\theta}\frac{\partial}{\partial\phi}(\rho w)=0$$

Presented as Paper 78-1358 at AIAA Atmospheric Flight Mechanics Meeting, Palo Alto, Calif., Aug. 7-9, 1978; submitted June 20, 1980; revision received Dec. 11, 1980.

*Member of AIAA.

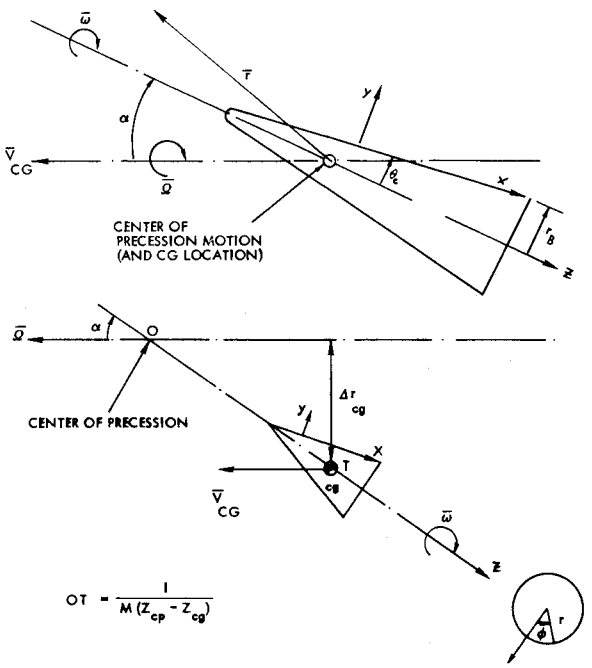

Fig. 1 a) Coordinate system (precession about center of gravity); b) coordinate system.

Momentum:

$$\rho\frac{Du}{Dt}+2\rho(w\Omega_2-v\Omega_3)-\frac{\rho}{r}(v^2+w^2)$$
$$+\rho l_2\Omega_1\Omega_2-\rho l_1(\Omega_2^2+\Omega_3^2)+\frac{\partial p}{\partial r}=0$$
$$\rho\frac{Dv}{Dt}+\frac{\rho uv}{r}-\frac{\rho w^2\cot\theta}{r}+2\rho(u\Omega_3-w\Omega_2) \tag{2}$$
$$-\rho l_2(\Omega_1^2+\Omega_3^2)+\rho l_1\Omega_1\Omega_2+\frac{1}{r}\frac{\partial p}{\partial\theta}=0$$

and

$$\rho\frac{Dw}{Dt}+\frac{\rho uw}{r}+\frac{\rho vw}{r}\cot\theta+2\rho(v\Omega_1-u\Omega_2)$$
$$+\rho[l_1\Omega_1\Omega_3+l_2\Omega_2\Omega_3]+\frac{1}{r\sin\theta}\frac{\partial p}{\partial\phi}=0$$

The equation of state:

$$\rho\frac{Ds}{Dt}=0$$

where

$$\frac{D}{Dt}=\frac{\partial}{\partial t}+u\frac{\partial}{\partial r}+\frac{v}{r}\frac{\partial}{\partial\theta}+\frac{w}{r\sin\theta}\frac{\partial}{\partial\phi}$$

The (u,v,w) and $(\Omega_1,\Omega_2,\Omega_3)$ are the translational and angular velocities in (r,θ,ϕ) direction, respectively. The constants $l_1,l_2,\hat{Z}$ and Z_{cg} are defined as $l_1=-\hat{Z}\cos\theta-r\sin^2\theta$; $l_2=\hat{Z}\sin\theta-r\sin\theta\cos\theta$; $\hat{Z}=r\cos\theta+|Z_{cg}|$; Z_{cg} = axial location of center of gravity.

An independent variable transformation

$$\zeta=(r-r_w)/(r_s-r_w),\quad t=t,\quad \phi+\phi,\quad \theta=\theta$$

normalizes the wall-to-shock distance. The outer boundary conditions at the shock are the Rankine-Hugoniot conditions with the freestream velocity defined as

$$\vec{v}_\infty=-\vec{v}_{cg}+\Omega\times r \tag{3}$$

The bow-shock envelopes are allowed to relax until steady-state solutions are obtained. Herein, a modified method of the characteristic[8] is employed to update the shock movement. The wall boundary points are satisfied by imposing $V\cdot n=0$ (where n is the surface normal vector), and the surface pressure is calculated by a compatibility relation[7,8] along a characteristic in the (ζ,t) plane. Symmetry conditions are not invoked at the windward or leeward planes. Instead, continuity of the flow profiles at $\phi=0$ and 2π is imposed. The governing equations are integrated by MacCormack's two-level explicit scheme with the stability restriction dictated by the Courant-Frederick-Levy rule.

Outer Inviscid Flows—Supersonic-Flow Region

The basic equations for supersonic flow are written in cylindrical coordinates[7] (see Fig. 1):

$$E_z+F_\eta+G_\phi+H=0$$

where

$$E=\begin{bmatrix}\rho u\\ p\epsilon+\rho u^2\\ \rho uv\\ \rho uw\end{bmatrix}\qquad F=\begin{bmatrix}\rho D\\ \rho uD-p\epsilon\eta_z\\ \rho vD+p\epsilon\eta_r\\ \rho wD+\dfrac{p\epsilon}{r}\eta_q\end{bmatrix}$$

$$G=\begin{bmatrix}\dfrac{\rho v}{r}\\ \dfrac{\rho uw}{r}\\ \dfrac{\rho vw}{r}\\ (\rho\epsilon+\rho w^2)\dfrac{1}{r}\end{bmatrix}$$

and

$$H=A_1E+A_2G+\begin{bmatrix}\dfrac{\rho v}{r}\\ \dfrac{\rho uv}{r}+\Lambda_1\\ \dfrac{\rho}{r}(v^2-w^2)+\Lambda_2\\ \dfrac{2\rho vw}{r}+\Lambda_3\end{bmatrix} \tag{4}$$

where

$$\eta=(r-r_w)/(r_s-r_w),\qquad \epsilon=(M_\infty^2\gamma)^{-1}$$
$$A_1=(r_{s_Z}-r_{w_Z})/\Delta,\qquad \Delta=r_s-r_w$$
$$A_2=(r_{s_\phi}-r_{w_\phi})/\Delta$$
$$D=u\eta_Z+v\eta_r+\frac{w}{r}\eta_\phi$$
$$\Lambda_1=\rho[2B(\sin\alpha\cos\phi w+v\sin\alpha\sin\phi)-B^2Z\sin^2\alpha$$
$$-rB^2\cos\alpha\sin\alpha\cos\phi]$$
$$\Lambda_2=\rho[2B(w\cos\alpha-u\sin\alpha\sin\phi)$$
$$-ZB^2\cos\alpha\sin\alpha\cos\phi-rB^2\sin^2\alpha]$$
$$\Lambda_3=\rho[2B(-v\cos\alpha-u\sin\alpha\cos\phi)$$
$$+ZB^2\cos\alpha\sin\alpha\sin\phi-rB^2\sin^2\alpha\sin\phi\cos\phi]$$
$$B=L\Omega/u_\infty$$

The matrix F is expressed in terms of p and D which are slow-varying functions across a vortex sheet (e.g., $D=0$ at $r=r_w$).

This is significant when one takes the η-derivative across a thin entropy layer existing on a blunt slender cone.

For missiles in coning motion, the energy equation can be written

$$p=\rho\left\{1+\left(\frac{\gamma-1}{2}\right)M_\infty^2\left[1-\frac{u^2+v^2+w^2}{U_\infty^2}\right]+\frac{\gamma-1}{2}M_\infty^2B^2 + \left[\frac{Z^2\sin^2\alpha}{L^2}+\frac{r^2}{L^2}(\cos^2\alpha+\sin^2\alpha\sin^2\phi)+\frac{rZ}{L^2}\sin 2\alpha\cos\phi\right]\right\} \tag{5}$$

The boundary conditions, numerical integration algorithm, and stability criterion are similar to the blunt-body time-dependent calculations discussed previously, except that the timewise coordinate is the Z axis in the supersonic-flow computations. Modifications have been made with the derivatives. At windward and leeward meridian, central differences are applied. For 0 deg $<\phi<$ 180 deg, forward differencing is used in the predictor and backward differencing in the corrector. The order of differencing is reversed for 180 deg $<\phi<$ 360 deg. This modification helps preserve the natural symmetry in the flowfields as $\Omega\to 0$.

Inner Viscous Flow[7,9]

The conventional boundary-layer equations are modified to include pertinent effects of crossflow diffusion, centrifugal force, and Coriolis accelerations. With the usual boundary-layer approximation $\partial/\partial y \gg \partial/\partial x$, $Re\gg 1$ and the retention of crossflow diffusion terms which are required to adequately describe boundary regions or local shear flows formed near separation plane so that $(1/r)(\partial/\partial\phi)=0(\partial/\partial y)$ locally, the Navier-Stokes equations in body-oriented coordinates reduce to (see Fig. 1):

Continuity:

$$(\rho u)_x+(\rho v)_y+\frac{1}{r}[\rho u\sin\theta+\rho v\cos\theta+(\rho w)_\phi]=0$$

Momentum:

$$\rho uu_x+\rho vu_y+\frac{\rho w}{r}u_\phi-\frac{\rho w^2}{r}\sin\theta+p_x +2\rho(w\Omega_2-v\Omega_3)+\rho\Omega_2(x_2\Omega_1-x_1\Omega_2) -x_1\Omega_3^2=\frac{1}{r}\frac{\partial}{\partial y}(\mu ru_y)+\frac{1}{r^2}\frac{\partial}{\partial\phi}(uu_\phi)$$

$$p_y=\frac{\rho w^2\cos\theta}{r}-2\rho(u\Omega_3-w\Omega_1)+\rho x_2\Omega_3^2 +\rho\Omega_1(x_2\Omega_1-x_1\Omega_2)$$

and

$$\rho uw_x+\rho vw_y+\frac{\rho w}{r}w_\phi+\frac{\rho uw}{r}\sin\theta +\frac{\rho vw}{r}\cos\theta+\frac{1}{r}p_\phi+2\rho(v\Omega_1-u\Omega_2) +\rho x_1\Omega_1\Omega_3+x_2\Omega_2\Omega_3\rho =\frac{1}{r}\frac{\partial}{\partial y}(\mu rw_y)+\frac{4}{3r^2}\frac{\partial}{\partial\phi}(\mu w_\phi)$$

Energy:

$$\rho uT_x+\rho vT_y+\frac{\rho w}{r}T_\phi +p\left[U_x+V_y+\frac{u\sin\theta+v\cos\theta+w_\phi}{r}\right] -\rho u\Omega_2(x_2\Omega_1-x_1\Omega_2)+\rho ux_1\Omega_3^2-\rho wx_1\Omega_1\Omega_3-\rho wx_2\Omega_2\Omega_3 =\frac{1}{r}\frac{\partial}{\partial y}(KrT_y)+\frac{1}{r^2}\frac{\partial}{\partial\phi}(KT_\phi)+\mu(u_y^2+w_y^2) +\frac{1}{r^2}\left[\mu\left(u_\phi^2+\frac{4}{3}w_\phi^2+w^2\cos\theta\right)\right] \tag{6}$$

where

$$x_1=x-x_{cg},\qquad x_2=y+y_{cg}$$

and (u,v,w) and $(\Omega_1,\Omega_2,\Omega_3)$ are the translational and angular velocity in the (x,y,ϕ) direction, respectively. The coordinate system is attached to the cone surface and does not spin with the body. The governing system is not restricted to small crossflow. The retention of azimuthal diffusion terms has been found to be significant such that the secondary-flow separation line is not a singular point in this formulation.

The boundary conditions for the viscous flow are

$$y=0,\quad u=v=0,\quad w=r_w\omega,\quad T=T_w\quad\text{or}\quad T_y=0$$

$$y=\delta,\quad u=U_e,\quad w=w_e,\quad T=T_e$$

The boundary-layer edge properties are acquired from the inviscid-flow solutions. In order to account for the entropy-layer swallowing effects, one can obtain the edge properties from the inviscid-flow profile, at a distance $\delta-\Delta^*$ from the surface. Here δ is the boundary layer thickness and Δ^* is the three-dimensional viscous displacement thickness defined as

$$\frac{\partial}{\partial x}[\rho_e u_e r(\Delta^*-\delta_1^*)]+\frac{\partial}{\partial\phi}[\rho_e w_e(\Delta^*-\delta_2^*)]=0$$

where

$$\delta_2^*=\int_0^\delta\left(1-\frac{\rho w}{\rho_e w_e}\right)dy$$

$$\delta_1^*=\int_0^\delta\left(1-\frac{\rho u}{\rho_e u_e}\right)dy$$

Once again the windward and leeward surfaces are not symmetry planes for the spinning and precessed cone; rather, a periodic continuation of the flow profiles at $\phi=0$ and 2π is specified.

Both laminar and turbulent flows are included in the numerical model. Cebeci's two-layer algebraic eddy viscosity model[7] with transverse-curvature and pressure-gradient corrections is employed herein. The basic equations are integrated by an iterative implicit scheme with the marching step, Δx, limited by

$$\Delta x<\frac{u}{w}(r\Delta\phi) \tag{7}$$

Initial conditions are obtained from blunt-body boundary-layer calculations. Blottner's formulation[7] is used herein for the nosetip region, and the detailed analysis is given in Ref. 7. The inner-viscous-flow and outer-inviscid-streams calculations are coupled in a manner similar to Prandtl's classical boundary-layer theory. Simultaneous numerical integration of these two distinct regions are made.

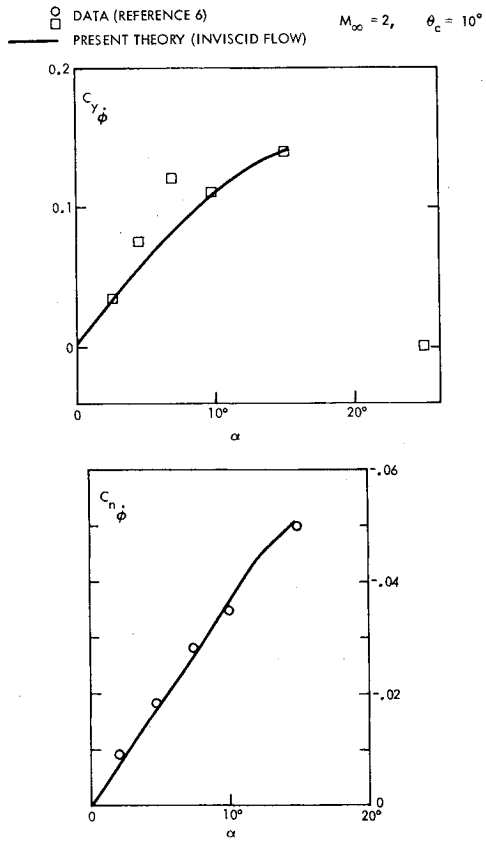

Fig. 2 Side-force and side-moment coefficients distributions.

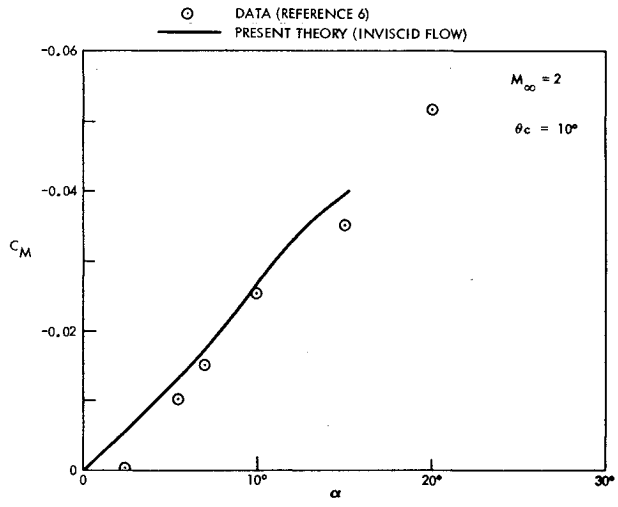

Fig. 3 C_M vs α.

Results and Discussion

Inviscid Flow Results

Numerical results have been obtained on a sharp cone in the $M_\infty = 2$ flow which correspond to Schiff and Tobak's coning experiments.[6] Figure 2 depicts the induced side-force coefficient and side-moment coefficient due to coning motion. The data, also shown in the figure for comparison, indicate a nonlinear distribution with angles of attack when $\alpha/\theta_c > 1.2$. The variation of pitching moment with the angle of attack on a pointed cone is given in Fig. 3. At each α, no change in C_m was noted as the coning rate parameter $B = L\Omega/U_\infty$ was varied. Therefore, the coning motion has negligible effects on the pitching moment.

There are some scatterings in Schiff and Tobak's data (e.g., C_m does not approach zero as $\alpha \to 0$). This occurs because the

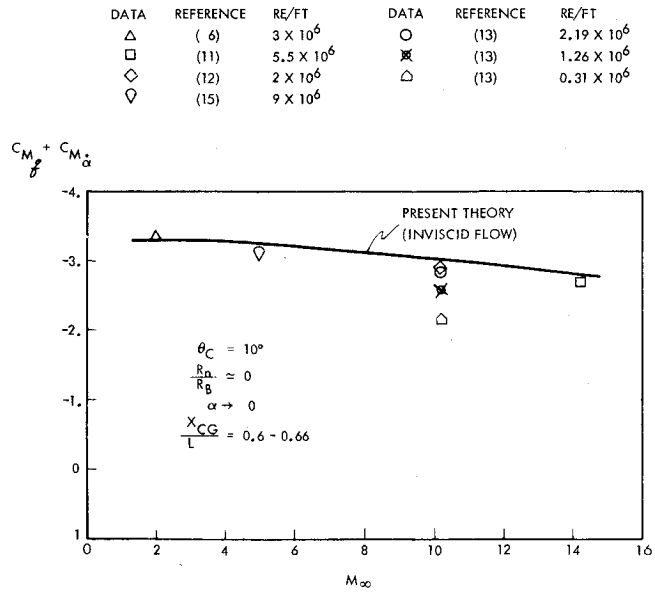

Fig. 4 Variation of pitch-damping derivative with Mach number.

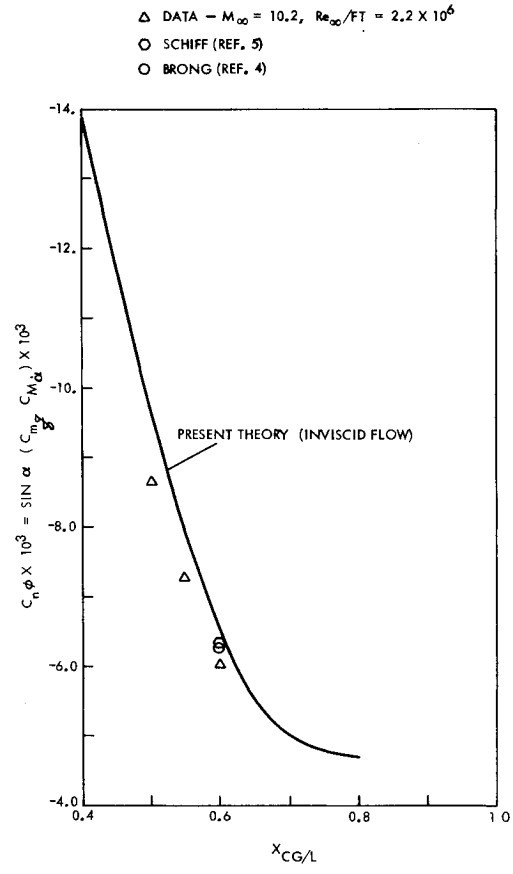

Fig. 5 Variation of side-moment coefficient with the center-of-gravity location.

centrifugal tare loads caused by the coning motion are of the same order as the aerodynamic loads.[6] However, the centrifugal loads affect only the C_N and C_m, not the side force and moment.

Tobak and Schiff[10] have demonstrated that the complete specification of the moments acting on a body in a general nonplanar motion requires knowledge of moments acting on the body in four characteristic motions: steady angle of attack, damping in pitch, damping in roll, and coning motion. Furthermore, they have shown that for a body of revolution at a small angle of incidence, a calculation of $C_{n_{\dot\phi}}$ would be

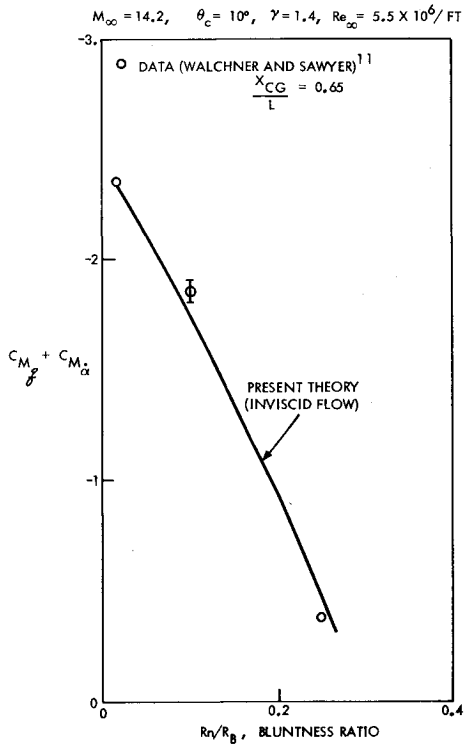

Fig. 6 Dynamic-moment coefficient vs bluntness ratio.

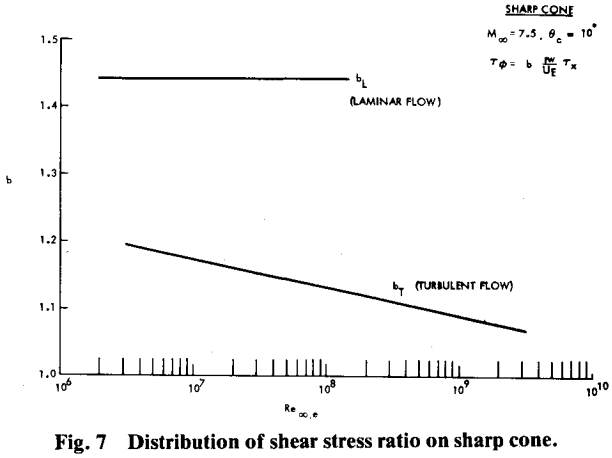

Fig. 7 Distribution of shear stress ratio on sharp cone.

equivalent to a calculation of the linear damping in pitch, i.e.,

$$C_{n_{\dot\phi}} = \sin\alpha[C_{m_q} + \cos\alpha C_{m_{\dot\alpha}}] \doteq \sin\alpha[C_{m_q} + C_{m_{\dot\alpha}}], \quad \alpha \to 0 \quad (8)$$

Therefore, coning motion, wherein the nose of the vehicle describes a circle around the flight velocity vector, has a particular significance because the side-moment coefficient acting on the body at small angle of attack can be related to the linear damping in pitch derivatives. Figure 4 shows the $C_{m_q} + C_{m_{\dot\alpha}}$ variation with freestream Mach number. Comparison is made with wind-tunnel results.[6,11-13,15] Note that as M_∞ increases, the pitch-damping derivative starts to decrease. However, the data obtained at $M_\infty = 10.2$ (Ref. 13) indicates that $C_{m_q} + C_{m_{\dot\alpha}}$ falls off rapidly as the Reynolds number decreases.† This suggests that the stability of a cone is greatly

†Ballistic range data (Ref. 14) reports an increase in dynamic stability as M_∞ is increased. However, Jaffe and Preslin's free-flight measurements (Ref. 16) indicate that $-(C_{m_q} + C_{m_{\dot\alpha}})$ decreases as M_∞ increases.

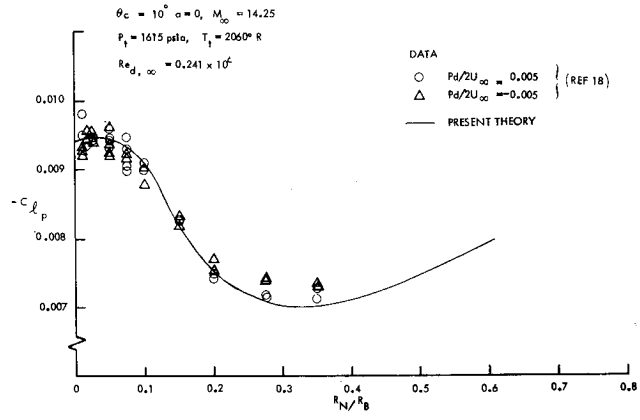

Fig. 8 Laminar-flow roll-damping derivative vs bluntness ratio.

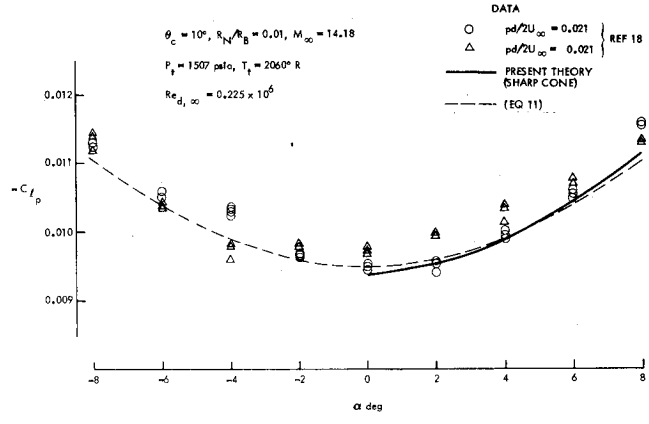

Fig. 9 Sharp-cone laminar-flow roll-damping derivative vs angle of attack.

reduced under low-Reynolds-number conditions. This effect, presumably viscous, needs further experimental verification. The present numerical results compare favorably with high-Reynolds-number experimental data.[6,11-13]

The effects of varying the center of gravity or oscillation pivot location are shown in Fig. 5. A large variation in pitch damping with center of gravity location on a sharp cone is noted. The numerical results compare reasonably well with the wind-tunnel data[13] of high Reynolds number.

The effects of increasing the nose bluntness on the dynamic pitch damping of a 10-deg cone are demonstrated in Fig. 6. Walchner and Sawyer's experimental measurements[11] are also given in Fig. 6 as a comparison. The general trend of our numerical results indicates a decrease in damping with an increase in nose bluntness.

Viscous-Flow Results[9]

The present coupled viscous- and inviscid-flow formulation can be easily used to evaluate the Magnus force in laminar, transitional, and turbulent flows. However, this paper concentrates on obtaining the roll-damping derivative which, along with the pitch-damping derivative, is one of the important parameters in RV roll-trim analysis.

The aerodynamic roll-damping moment on a slender vehicle is attributed entirely to viscous effects that tend to reduce the vehicle spin rate. The roll-damping derivative is defined as

$$C_{l_p} = -\frac{\int_0^s \int_0^{2\pi} r^2 \tau_\phi \, d\phi dx}{q_\infty AD(r_w\omega/U_\infty)} \quad (9)$$

where A represents the cone base area, D the vehicle base diameter, q_∞ the freestream dynamic pressure, ω the spin

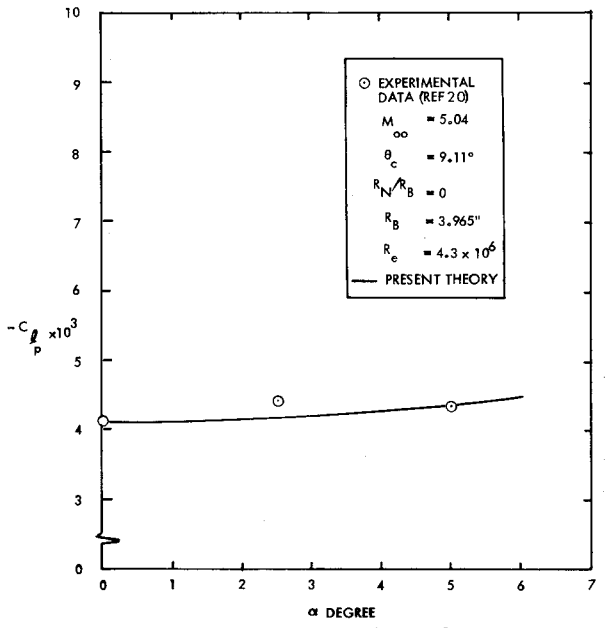

Fig. 10 Turbulent-flow roll damping on sharp cone.

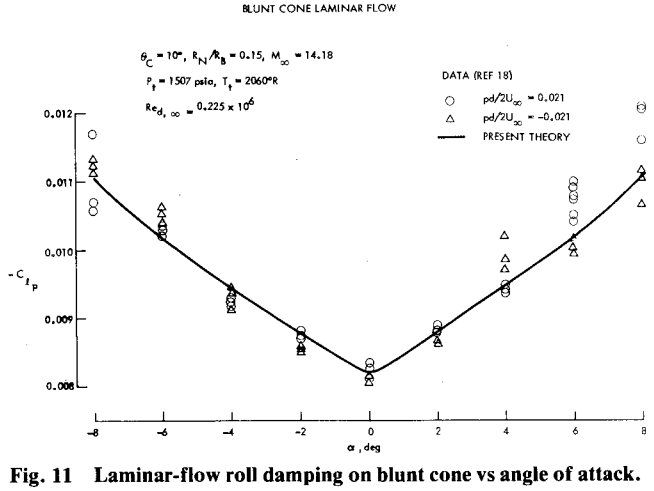

Fig. 11 Laminar-flow roll damping on blunt cone vs angle of attack.

rate, U_∞ the freestream velocity, and τ_ϕ the crossflow shear stress, i.e.,

$$\tau_\phi = \mu w_y \quad \text{at} \quad y=0$$

Numerical results for the ratio of τ_ϕ/τ_x (where τ_x is the main stream shear stress) on a spinning pointed cone at zero angle of attack are presented in a nondimensional form

$$\tau_\phi/\tau_x = b(r_w\omega/U_e) \tag{10}$$

and are given in Fig. 7. The parameter b assumes a constant value of 1.46 in laminar flow and is insensitive to Reynolds number, wall temperature, and cone angle. This is consistent with Illingsworth's analysis.[17] In turbulent flow, b is a weak function of the Reynolds number (see Fig. 7). Also, the numerical results indicate that τ_x is not affected significantly by spinning as long as $r\omega/U_e \ll 1$. The message obtained from Fig. 7 is that the crossflow drag on the spinning body can be accurately correlated with τ_x. This is useful since the streamwise shear stress usually can be accurately evaluated.

The effect of nosetip bluntness upon C_{l_p} is illustrated in Fig. 8 which shows that C_{l_p} decreases as r_N/r_B ratio increases. This trend continues until $r_N/r_B = 0.3$; then C_{l_p} starts to increase as r_N/r_B increases. This type of nonmonotonic

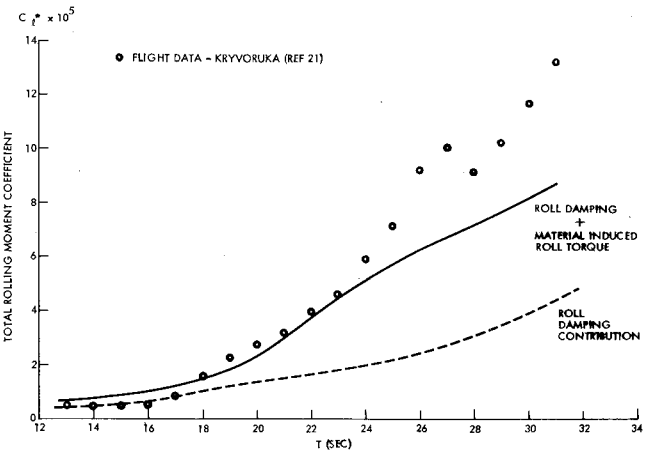

Fig. 12 RTE rolling-moment coefficient vs flight time.

distribution is caused by the surface-pressure overexpansion in blunt-cone configuration. The numerical results compare favorably with the experimental results of Walchner et al.[18] in laminar flow (Fig. 8).

The variation of laminar flow C_{l_p} for a sharp cone at angle of attack is depicted in Fig. 9. The general trend is that the roll-damping derivative increases as the angle of attack increases. An approximate solution for sharp-cone laminar flow C_{l_p} at angle of incidence can be derived as[19]

$$C_{l_p}/C_{l_{p0}} = 1 + \frac{1}{4}\left(\frac{\alpha}{\theta_c}\right)^2 + \cdots \tag{11}$$

where $C_{l_{p0}}$ is the roll-damping derivative at zero angle of attack. It is noted that Eq. (11) agrees well with Walchner's data[18] (see Fig. 9).

The turbulent flow C_{l_p} on a sharp cone at angle of attack is shown in Fig. 10. Herein, Cebeci's two-layer eddy viscosity model with transverse curvature effect is employed. The agreement between the experimental measurements[20] and the numerical results is reasonably good.

Finally, for a blunt cone at angle of attack, the laminar flow C_{l_p} is given in Fig. 11. It indicates that the roll-damping derivative increases more rapidly with angle of attack on a blunt cone than on a sharp cone. Again, the present numerical results agree favorably with the wind tunnel data.

The roll dynamics of a spinning vehicle can be written as

$$I\dot{\omega} = q_\infty AD\left[C_{l_0} - C_{l_p}\frac{r\omega}{U_\infty} + C_{N_\alpha}\alpha\left(\frac{\Delta\text{C.P.}}{D}\right)\right]$$

$$= q_\infty AD\left[C_l^* + C_{N_\alpha}\alpha\left(\frac{\Delta\text{C.P.}}{D}\right)\right]$$

where C_{l_0} = roll torque coefficient, $C_l^* = C_{l_0} - C_{l_p}(r\omega/U_\infty)$, and ΔC.P. = center of pressure offset.

Usually the roll-damping contribution is small, except at low altitude where ω is high and U_∞ is comparatively low. Then C_{l_p} contribution can become significant. One example is given in Fig. 12 which shows the flight data C_l^* for RTE vehicle.[21] Most analytical predictions without including the roll-damping contribution considerably underpredict the C_l^*. Therefore, the roll-damping contributions should be included in the flight simulation and data correlation.

Summary

Numerical results have been presented on the aerodynamics of a RV in steady coning motion. A brief summary is now given below.

Tobak and Schiff's relation[9] [i.e., Eq. (8)] can be used to calculate the pitch-damping derivative when $\alpha \to 0$. Herein, the

effects of freestream Mach number, bluntness ratio, and center of gravity location upon the $C_{m_q}+C_{m_{\dot{\alpha}}}$ are demonstrated.

The RV precession motion has a small effect on the normal force and pitch moment (i.e., C_N and C_m).

The RV side forces and moments induced by coning motion are essentially an inviscid-flow phenomenon. This is different from Magnus forces and moments[16] which are caused by asymmetric viscous displacement on a spinning cone at angle of attack.

Hobbs' wind-tunnel measurements[12] indicate that there are low Reynolds number effects on the $C_{m_q}+C_{m_{\dot{\alpha}}}$. Presumably, the viscous interaction phenomena are important. However, Jaffe and Preslin's data in the laminar-, transitional-, and turbulent-flow regimes show no obvious Reynolds-number effects. The present inviscid flow results on $C_{m_q}+C_{m_{\dot{\alpha}}}$ agree reasonably well with the high-Reynolds-number wind-tunnel measurements.

The laminar- and turbulent-flow roll-damping derivatives are estimated on a spinning cone. Effects of angle of attack and nosetip bluntness ratio are demonstrated.

Acknowledgment

This work was supported by the Air Force Ballistic Missile Office under Contract FO4704-80-C-0021.

References

[1] Marconi, F., Yeager, L., and Hamilton, H.H., "Computation of High Speed Inviscid Flows About Real Configurations," NASA-SP-347, March 1975, pp. 1411-1455; also see Hall, D.W. and Dougherty, C.M., Ballistic Missile Office Technical Report TR-80, June 1980.

[2] Kutler, P., Lomax, H., and Warming, R.F., "Computations of Space Shuttle Flow Fields Using Noncentered Finite-Difference Schemes," *AIAA Journal,* Vol. 11, Feb. 1973, pp. 196-204.

[3] Soloman, J.M. et al., "Three-Dimensional Supersonic Inviscid Flow Field Calculations on Reentry Vehicle with Control Surfaces," AIAA Paper 77-84, Jan. 1977.

[4] Brong, E.A., "The Flow Field About a Pointed Cone in Unsteady Motion in a Supersonic Stream," FDL-TDR-64-148, Dec. 1965.

[5] Schiff, L.B., "Computation of Supersonic Flow Fields About Bodies in Coning Motion Using a Shock-Capturing Finite-Difference Technique," AIAA Paper 72-27, 1972.

[6] Schiff, L.B. and Tobak, M., "Results From a New Wind-Tunnel Apparatus for Studying Coning and Spinning Motions of Bodies of Revolution," *AIAA Journal,* Vol. 8, Nov. 1970, pp. 1953-1958.

[7] Lin, T.C. and Rubin, S.G., "A Two-Layer Model for Coupled Three-Dimensional Viscous and Inviscid Flow Calculations," AIAA Paper 75-853, June 1975.

[8] Moretti, G. and Pandolfi, M., "Analysis of the Inviscid Flow About a Yawed Cone, Preliminary Studies," Polytechnic Institute of Brooklyn Aeronautic Laboratory Report 72-18, 1972.

[9] Lin, T.C. and Rubin, S.G., "Viscous Flow Over Spinning Cones at Angle of Attack," *AIAA Journal,* Vol. 12, July 1974, pp. 975-985.

[10] Tobak, M. and Schiff, L.B., "A Nonlinear Aerodynamic Moment Formulation and Its Implication for Dynamic Stability Testing," AIAA Paper 71-275, 1971.

[11] Walchner, O. and Sawyer, F.M., "In-Plane and Out-of-Plane Stability Derivatives of Slender Cones at Mach 14," ARL-73-0090, Air Force Systems Command, Wright-Patterson AFB, July 1973.

[12] Ward, L.K. and Mansfield, A.C., "Dynamic Characteristics of a 9-Degree Cone With and Without Asymmetries at Mach Number 10," AEDC-TR-70-1, March 1970.

[13] Hobbs, R.B., "Results of Experimental Studies of the Hypersonic Dynamic Stability Characteristics of a 10° Cone at M = 10," GE-TAC Data Memo 1:37, May 1964 (AEDC-VKF-Tunnel C).

[14] Welsh, C.G., Winchenbach, G.L., and Madagan, A.N., "Free Flight Investigation of the Aerodynamic Characteristics of a Cone at High Mach Number," *AIAA Journal,* Vol. 8, Feb. 1970, pp. 294-300.

[15] Morrison, A.M., Holmes, J.E., and Lawrence, W.R., "An Investigation of the Damping in Pitch Characteristic of a Ten-Degree Cone," NSWC/WOL/TR 75-84, June 1975.

[16] Jaffe, P. and Preslin, R.H., "Effect of Boundary Layer Transition on Dynamic Stability," *Journal of Spacecraft and Rockets,* Vol. 3, Jan. 1966, pp. 46-52.

[17] Illingsworth, C.R., "The Laminar Boundary Layer of a Rotating Body of Revolution," *Philosophical Magazine and Journal of Science,* Vol. 44, 1953, pp. 389-403.

[18] Walchner, O., Sawyer, F.M., and Durham, T.A., "Hypersonic Wind Tunnel Measurements of Roll Damping Derivatives for Cones," ARL-69-0170, Air Force Systems Command, Wright-Patterson AFB, Oct. 1969.

[19] Lin, T.C., "A Numerical Study of the Aerodynamics of a Reentry Vehicle in Steady Coning Motion," AIAA Paper 78-1358, Aug. 1978.

[20] Jemke, T., private communication (AEDC-VKF-Tunnel A), 1977.

[21] Kryvoruka, J.K., "Roll Torque Evaluation (RTE) Vehicle Post-Flight Test Report," Sandia Laboratories, SAND-76-8001, March 1976.